Near-infrared emitting single squaraine dye aggregates with large Stokes shifts

Near-Infrared Emitting Single Squaraine Dye Aggregate with large Stokes shift

G. M. Paternò[1], L. Moretti[2], A. Barker[1], C. D'Andrea[1,2], A. Luzio[1], N. Barbero[3], S. Galliano[3], C.Barolo[3,4], G. Lanzani[1,2] and F. Scotognella[1,2]

[1] Center for Nano Science and Technology@PoliMi, Istituto Italiano di Tecnologia, Via Giovanni Pascoli, 70/3, 20133, Milan, Italy

[2] Dipartimento di Fisica, Politecnico di Milano, Piazza Leonardo da Vinci 32, 20133 Milano, Italy

[3] Dipartimento di Chimica and NIS Interdepartmental and INSTM Reference Centre, Università degli Studi di Torino, Via Pietro Giuria 7, 10125 Torino, Italy

[4] ICxT Interdepartmental Centre, Università di Torino, Lungo Dora Siena 100, 10100 Torino, Italy

Abstract

The study of supramolecular interactions and aggregation behaviour of functional materials is of great importance to tune and extend their spectral sensitivity and, hence, improve the optoelectronic response of related devices. In this study, we resolve spatially and spectrally the absorption and emission features of a squaraine aggregate by means of confocal microscopy and absorption/photoluminescence spectroscopy. We observe that the aggregate affords both a broad absorption spectrum (centred at 1.85 eV and extending to 1.55 eV), likely originated by a dyes configuration with allowed J- and H- arrangements, and a strong and relatively narrow emission in the near-infrared (NIR) part of the spectrum (centred at 1.59 eV), with a remarkable Stokes shift of 0.26 eV that is among the largest exhibited by squaraine dyes. These peculiarities would be beneficial for extending the spectral sensitivity of photovoltaic/light-emitting diodes and electrochemical cells, and extremely appealing for possible applications of these aggregates as NIR fluorescent probes in biomedical applications.

lntroduction

The optical properties and aggregation behaviour of squaraine dyes (SQ) have attracted a wide research interest in recent years, owing to their effective application in dye-sensitised,[1-3] organic[4, 5] and perovskite solar cells,[6] as well as in organic light-emitting diodes (OLEDs) [7] and biomedical applications.[8, 9] In particular, given their relatively strong light absorption (E > 300000 mol^{-1} cm^{-1}) and emission features in the near-infrared (NIR) part of the spectrum, SQs represent a class of the materials well suited for harvesting/emitting photons in the NIR region.

In this context, supramolecular interaction[10] is another important factor that plays a prominent role in tuning the spectral response of organic functional materials and, hence, widening up their possible range of applications. For these reasons, the study of self-organisation, crystallisation and aggregation behaviour of a variety of functional materials and chromophores have become an important topic in recent years.[11-17] More specifically, SQ dyes show a strong tendency to form both J-type and H-type aggregates in solution[16], with the former featuring a significant bathochromic shift and enhancement of absorption and the latter a hypsochromic shift and decrease of absorption with the respect of the monomeric band. On the other hand, in solid state[18-21] the presence of polymorphic species results in the observation of a complex aggregation pattern that includes the coexistence of J-, H- and also "oblique aggregates" that lead to a splitting of the absorption band into two components around the monomer absorption, the so-called Davydov splitting.[22] Therefore, it is somehow difficult to investigate the various aggregation contributions at the micro/nanoscale and map out the molecular arrangement in solid state. The study of the intrinsic optical properties of aggregates in solid films and polycrystalline materials would be, in fact, of great practical interest for the effective utilisation of such dyes in OPVs, OLEDs, organic light-emitting electrochemical cells (OLECs)[23, 24] and biosensing/imaging. This can be more relevant, for instance, in OPVs for which blending with electron acceptor materials increases the degree of morphological complexity of the active layer, and usually leads to a more convoluted aggregation pattern of SQs[18, 25].

Herein, we report a study of a single micron-sized polycrystalline aggregate of a squaraine derivative, namely VG1 -C8, exhibiting large Stokes shift (0.26 eV) and a considerable spectral distance between excitation (2.18 eV) and emission (1.59 eV) energies that are among the highest reported for SQs[26]. By

probing the different domains of the aggregate and of the surrounding film by means of confocal microscopy we observed that the aggregate shows a spectrally extended absorption both on the lower and higher energy sides of the monomer peak, possibly due to the coexistence of both J- and H- aggregates or Davydov splitting. Interestingly, we found that the photoluminescence from the aggregate core is substantially shifted towards the NIR region (1.59 eV), suggesting that an appreciable fraction of the aggregate affords a highly emissive J- configuration. The broad absorption spectrum extending to 1.55 eV and the strong luminescence in the NIR would be highly desirable features for OPVs[5, 27] and OLED/LEC[28-31] respectively, and would be also ideal for possible applications in biosensing and bioimaging.[32]

Experimental

Synthesis

5-carboxy-2,3,3-trimethyl-1-octyl-3H-indol-1-ium iodide (VG1-C8) was synthesised as previously reported in the literature[1, 33].

Aggregates formation

The aggregates, with sizes ranging from 20 μm to 80 μm, formed spontaneously upon increase of the concentration (10 mg/mL, 1.4 mM) in ethanol. To investigate the properties of those aggregates, we drop-cast the obtained dispersion, which contained both the aggregates and the saturated solution. This allowed us to study both the aggregate and the surrounding film.

Atomic force microscopy and X-rays diffraction

The surface topography of the aggregates and films were measured with an Agilent 5500 Atomic Force Microscope operated in the acoustic mode. X-ray diffraction measurements were carried out with a Bruker D8 advance in a thin film 28 scan model geometry, by using a Ka wavelength emitted by a Cu anode (0.15418 nm, 40 kV).

Confocal absorption and photoluminescence

The set-up consisted of a homemade microscope in transmission configuration, equipped with an 100x objective with NA of 0.7. The probe and excitation light came from a NKT Photonics SuperK Select laser,

continuously tunable from 475 to 1050 nm. The transmitted light was detected with an optical fibre connected to a silicon-based photodiode. Transmittance was calculated as $T = I/I_0$ by recording I_0 in a featureless region, and in the region of interest. Light transmission and photoluminescence were spatially resolved by raster-scanning the sample with respect to the laser beam through a piezo stage (P-517 Physik Instrumente) in x-y plane, with the z excursion used to optimise the focus on the sample. Transmission maps were taken at 500 nm, 690 nm and 880 nm, while localised transmission spectra were collected by scanning the laser emission wavelength. Photoluminescence (PL) measurements were performed by exciting the sample at 570 nm (2.18 eV). The collected PL wavelength was selected by inserting low-pass (LP) or band pass (BP) filters between the sample and the optical fibre coupler, enabling the collection of PL maps that spatially resolve different aggregate emissions. Localised PL spectra were recorded by coupling the collection fibre to an Ocean Optics Maya2000 Pro spectrometer, using a 600 nm (2.07 eV) LP filter to remove the residual excitation light.

Time-resolved photoluminescence

Ti:sapphire tunable laser source (Coherent Chameleon Ultra II) emits a train of light pulses operating at a repetition rate of 80 MHz with a temporal bandwidth of about 150 fs. Samples were excited at 520 nm by tuning the central wavelength of the laser at 1040 nm and frequency doubling it with a 1-barium borate crystal. In order to acquire the fluorescence signal on the aggregates a home-built micro-fluorimetry set up has been adopted. In particular an epi-fluorescence geometry was used, together with a 20x objective (Zeiss, Germany) obtaining a spot-size of about 3 μm (FWHM). By means of a spectrometer (Princeton Instruments, USA) the fluorescence emitted from the samples and collected by the microscope was dispersed and then coupled to a Streak Camera detection system (C5680 Hamamatsu, Japan) for the acquisition of spectrally- and time-resolved curves.

Results and discussion

Figure 1 summarises the main molecular and optical properties of VG1-C8, alongside with a visual description of the aggregates formation. The absorption spectrum of VG1-C8 in dilute solution (0.1 mg/mL, 0.14 mM) shows a strong and narrow band at 645 nm that can be attributed to the n → n* transition, and its vibronic shoulder at 600 nm.[3] The small Stokes shift of VG1-C8 (0.02 eV) is typical for symmetric squaraine derivatives, and it is indicative of comparable molecular configuration between the ground and excited electronic states of the molecule.[34, 35] Interestingly, we noticed the spontaneous formation of shiny golden aggregates upon increase of the concentration to 10 mg/mL (14.03 mM) in ethanol (fig. 1c). We therefore drop-cast the VG1-C8 aggregates dispersed in the ethanol solution on a glass substrate, in order to proceed to the morphological/structural and spectroscopic investigation of the squaraine aggregate and the surrounding film. The sizes of such aggregates range from 20 μm to 80 μm as measured by optical microscopy (fig. 1d) and thickness from ;: 200 nm to ;: 450 nm (by profilometry, see figure S1).

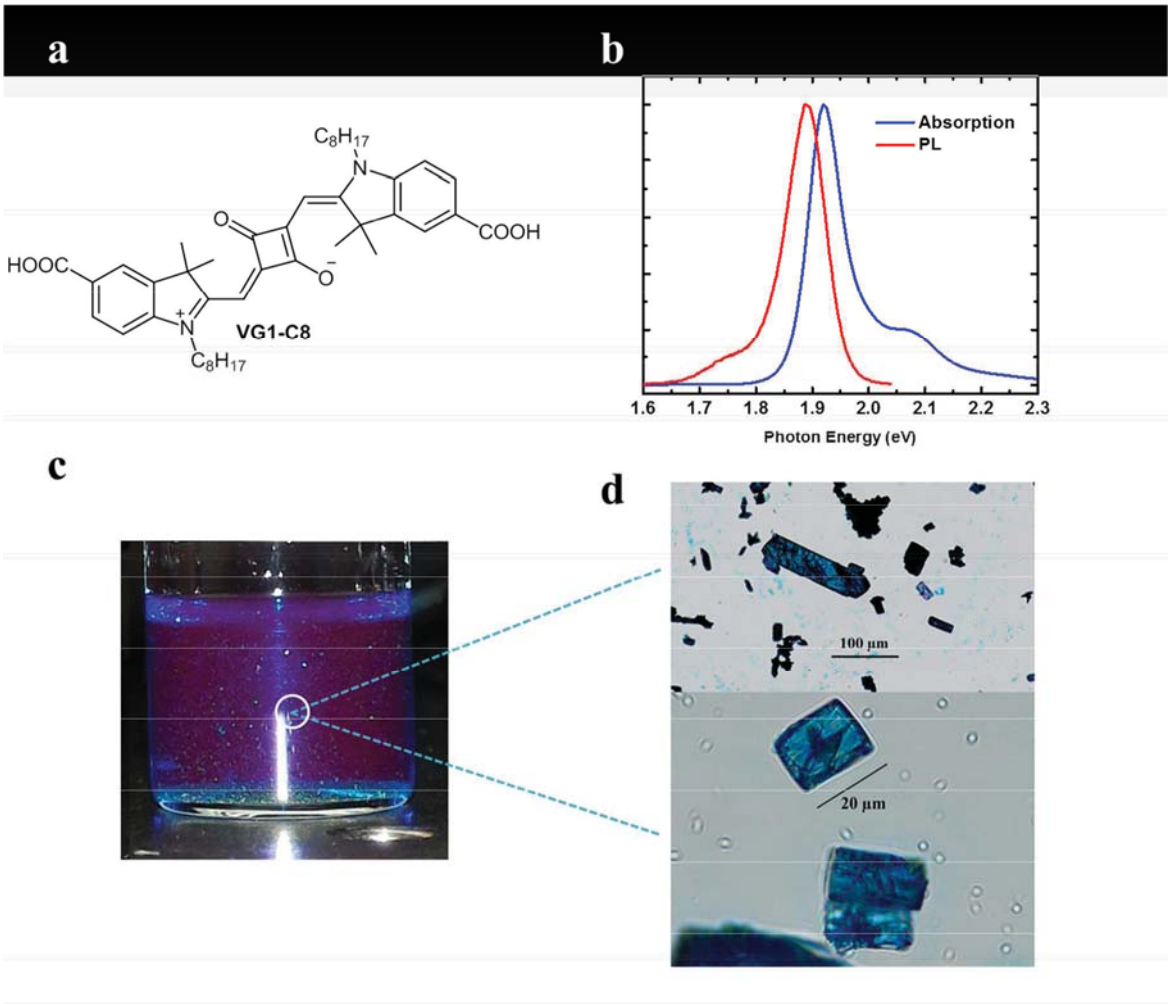

Figure 1. (a) Molecular structure of VG1-C8; (b) Normalised UV-Vis absorption and photoluminescence spectra of VG1-C8 in ethanol solution (0.1 mg/mL); (c) spontaneous formation of shiny and aggregates in a 10 mg/mL ethanol solution of the dye; (c) optical microscope images of the aggregates drop-cast on a glass substrate.

Hence, we combined atomic force microscopy (AFM) and x-ray diffraction (XRD) to obtain further details about the intrinsic structural/morphological features of such objects, with the view to understand better their optical characteristics. The AFM images taken on the surface of the aggregate (figure 2a height, 2b phase) reveal a rough and uneven surface that can be compatible with a polycrystalline arrangement of the aggregate. For comparison, we also performed AFM measurements on the surrounding film (see figure S2) that highlights the different nature of the two domains, with the film displaying a homogeneous and relatively smooth surface (mean square roughness 1.4 nm). The deep difference between the aggregate and the film morphologies stems from the different mechanism and time of solidification: whereas the slow

formation of aggregates in solution leads to bulky and polycrystalline objects, the relatively quick evaporation of the solvent (ethanol, T_b = 78.4 °C) leads to a more homogeneous and thin film-like morphology. Interestingly, the aggregate surface featured recurrent height values multiples of either 2.5 nm and 3 nm as calculated by AFM height-profile (figure 3c). Such height values might be compatible with one of the unit-cell parameters found in similar symmetric SQs derivatives (20-30 nm),[27, 36] although further structural experiments would be necessary to validate fully these findings. To finalise the structural/morphological characterisation of SQs aggregates and film, we carried out x-ray diffraction on the drop-cast aggregates and films along the out-of-plane direction. The XRD pattern (figure 2d) shows a marked difference between the aggregates and film signals, with the aggregates featuring a reflection at d-space of 8.6 A and the film showing a peak at a sensibly longer d-space (28.5 A). The former peak can be associated with the reflection from the (003) plane observed in powder diffraction analysis of VG1-C8,[37] whereas the rather expanded d-space found in film can be linked to the edge-on stacking of the molecule in the out-of-plane direction. We anticipate that the higher degree of intermolecular arrangement in the aggregate would also explain the peculiar optical features exhibited by those polycrystalline objects in comparison with the surrounding film.

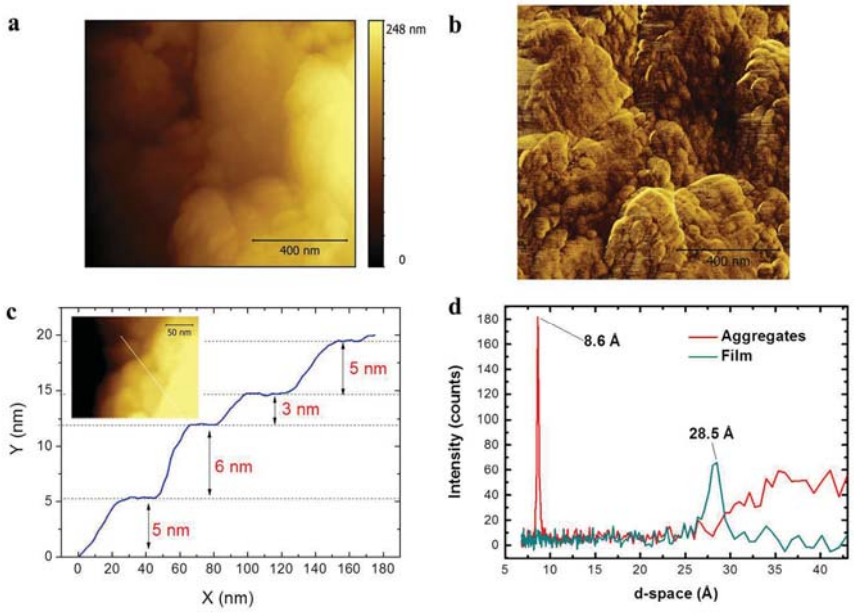

Figure 2: (a) AFM height and (b) phase images taken on top of a VG1-C8 aggregate; (c) AFM height-analysis of the aggregate surface; (d) out-of-plane XRD pattern of the VG1-C8 aggregate (red curve) and film (cyan curve).

In figure 3a-f we show the confocal transmission and PL maps of the aggregate. To acquire preliminary information about the transmission and PL spectral shape of the aggregate, we sampled the transmission at 500 nm (2.48 eV), 690 nm (1.8 eV) and 800 nm (1.55 eV), and the PL at 650 nm (1.91 eV), 750 nm (1.65 eV) and 800 nm (1.55 eV) by using band-pass filters centred in those wavelengths (FWHM 10 nm). Starting from the transmission maps, we can observe that the position of the absorption peak is roughly centred at the same wavelengths of the solution absorption, even though the aggregate shows an extended transmission spectrum both at the lower (fig. 3a) and higher (fig. 3c) sides of the peak. We also note a decrease of the transmission in the area all-surrounding the aggregate that we attribute to the VG1-C8 film. Interestingly, the PL maps taken at 650 nm, 750 nm and 800 nm permit us to distinguish spatially three regions with strongly different spectral emission properties. In particular, by probing the PL at 650 nm (1.91 eV) we collect the fluorescence in the low-Stoke shift regime, which in our case comes mostly from the surrounding film. On the other hand, at 750 nm (1.65 eV) and 800 nm (1.55 eV) we sample mainly the emission from the border and the centre of the aggregate, respectively.

To summarise this section, the confocal transmission maps show an extended and broad absorption spectrum of the polycrystalline aggregate, which might be attributed to both intermolecular charge-transfer interactions in the solid state[25, 38] and/or to the presence of different domains with mixed J- and H- character. The PL maps, interestingly, show that emission from the aggregate is markedly red-shifted with the respect of the surrounding film, corroborating the higher order of intermolecular interactions than in film as revealed by AFM and XRD analysis.

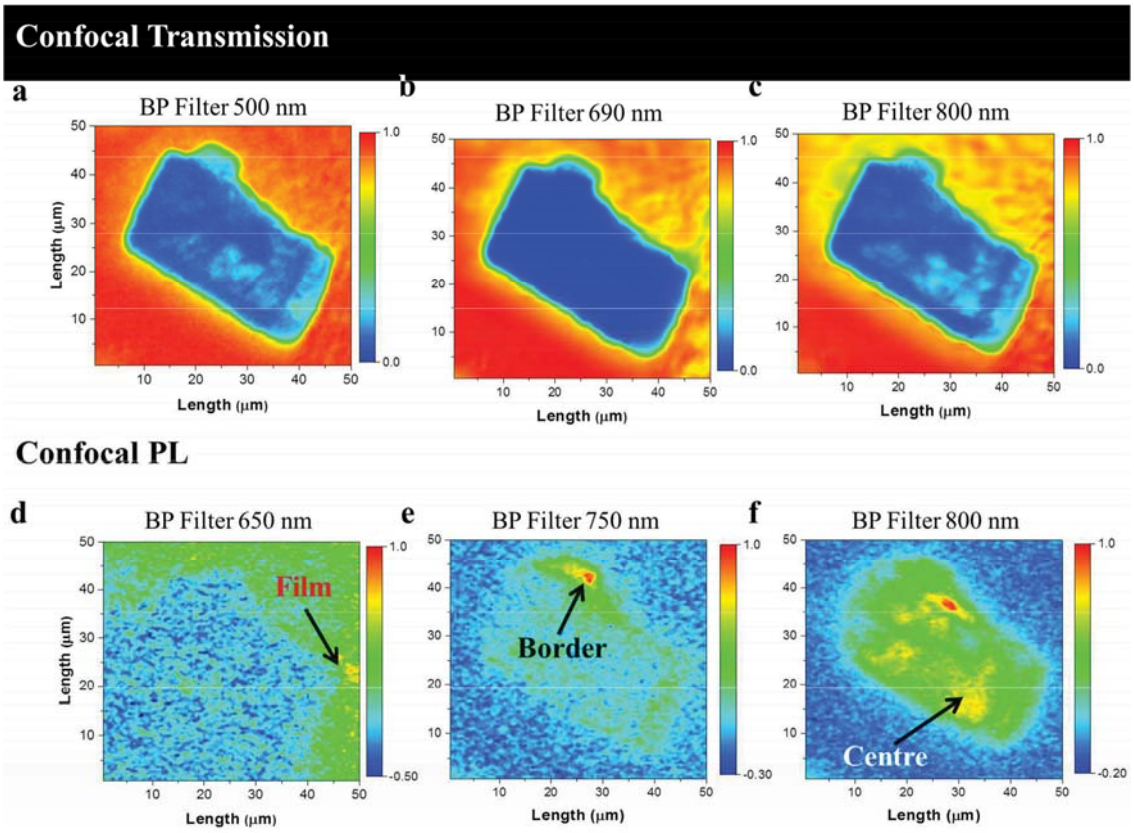

Figure 3: Normalised transmission (a-c) and PL (d-f) maps of the VG1 - aggregate (thickness **::** 160 µm as measured by profilometry) and surrounding film (thickness **::** 45 nm**)** . We employed BP filters to resolve spatially and highlight the different spectral contributions.

Figure 4a-b shows the local normalised absorption (4a) and PL (4b) spectra taken in the three different regions (film, border and centre, see the arrows in figure 3d-f), as well as the absorption/PL spectra of the solution for comparison. We can note that the absorption of the film is broader and blue-shifted with respect of the solution spectrum, although still overlapping with the solution monomeric absorption (39 % of the total integrated area). We attribute this to a distribution of species namely: monomers, H-aggregates and possibly a low fraction of J- aggregates that could be below the sensitivity of our absorption measurements. If we pass to the border of the aggregate, we still see a blue-shift of the spectrum and an enhanced absorption at higher energy, which can be connected to the presence of a mixed region with a higher molecular disorder at the edge of the aggregate (i.e. a higher fraction of grain boundaries and molecular misalignment)[39] and to the generation of H-type species. However, we also observe that the overlap between the edge and

monomeric absorption is considerably less than the previous case (27 %) and, in addition, there is the appearance of a new red-shifted band at 1.86 eV that can be a signature of an increased population of J-aggregates. Such findings may indicate that the fraction of monomeric VG1-C8 is substantially decreased at the expense of new generated H- and, to lower extent, J-aggregates. The scenario proposed above for the aggregate-edge lies somewhere in between the film and the aggregate core, as if we record the absorption spectrum at the centre we note that the monomeric peak lies almost in between the broad peak of the aggregate, which is concomitant with a decrease of the overlap with the monomeric band (24%). This can be linked to the coexistence of both J-type and H-type aggregates domains, or a dye arrangement that allows both J and H transitions (Davidov splitting).[18, 39] This feature, in particular, can be highly desirable for OPVs as it permits to extend the absorption cross section to the NIR region.

The PL spectra (fig. 4b), interestingly, seem to corroborate the aforementioned absorption results. In particular, the PL of the film is considerably overlapping with the solution emission (57 %), indicating the presence of a large fraction of monomeric species. However, we can note a slight red-shift of the emission (30 meV) and the appearance of a broad spectral feature lying at 1.69 eV (FWHM 300 meV, for the Gaussian fittings see figure S3) that can be attributed to a higher intermolecular order in the film and to the presence of J-aggregates, respectively. With regards to the aggregate-border, we observe the dramatic decrease of the monomeric peak together with the relative increase and narrowing of the component at 1.65 eV (FWHM 100 meV), which is consistent with the formation of emissive J-aggregates at the expenses of the monomeric form (24 % overlap). Remarkably, the aggregate core exhibits a mono-component, narrower and further red-shifted peak (1.59 eV, FWHM 90 meV) with a negligible overlap with the solution emission (5 %), indicating that the vast majority of the species is aggregated and, in particular, a significant fraction of these present a highly emissive J- configuration. The PL time-decay profiles of the aggregate and film (figure S3) show both a short and longer time-decay component (;: 39 ps and 1.5 ns, see figure S3), with the former being compatible with an increased radiative constant typical of J-aggregates,[40, 41], and the latter approaching the longer lifetimes of monomeric VG1-C8 in solution (1 - 2 ns).[34] Interestingly, however, we note that the amplitude of the long time-constant is considerably higher in the film (38%) than in the aggregate core (5%), confirming the higher amount of J-aggregates in our polycrystalline system than in the surrounding film.

It is worth saying that the absolute amount of absorbed/emitted light within the aggregate will be dependent on the absorption cross sections and PL relative quantum yields of the different domains, as well as to thickness fluctuations within the aggregate (see for example the AFM analysis in figure 2) and self-absorption phenomena. Those effects in-fact hinder a quantitative characterisation of the absorption/emission properties of the aggregate, even though we consider that the profound spectral changes observed in the different domains, such as spectral shifts and variation of the relative magnitude of the various spectral components, are real and related to the different population of species (monomeric, H- and J- aggregates) in the investigated sample.

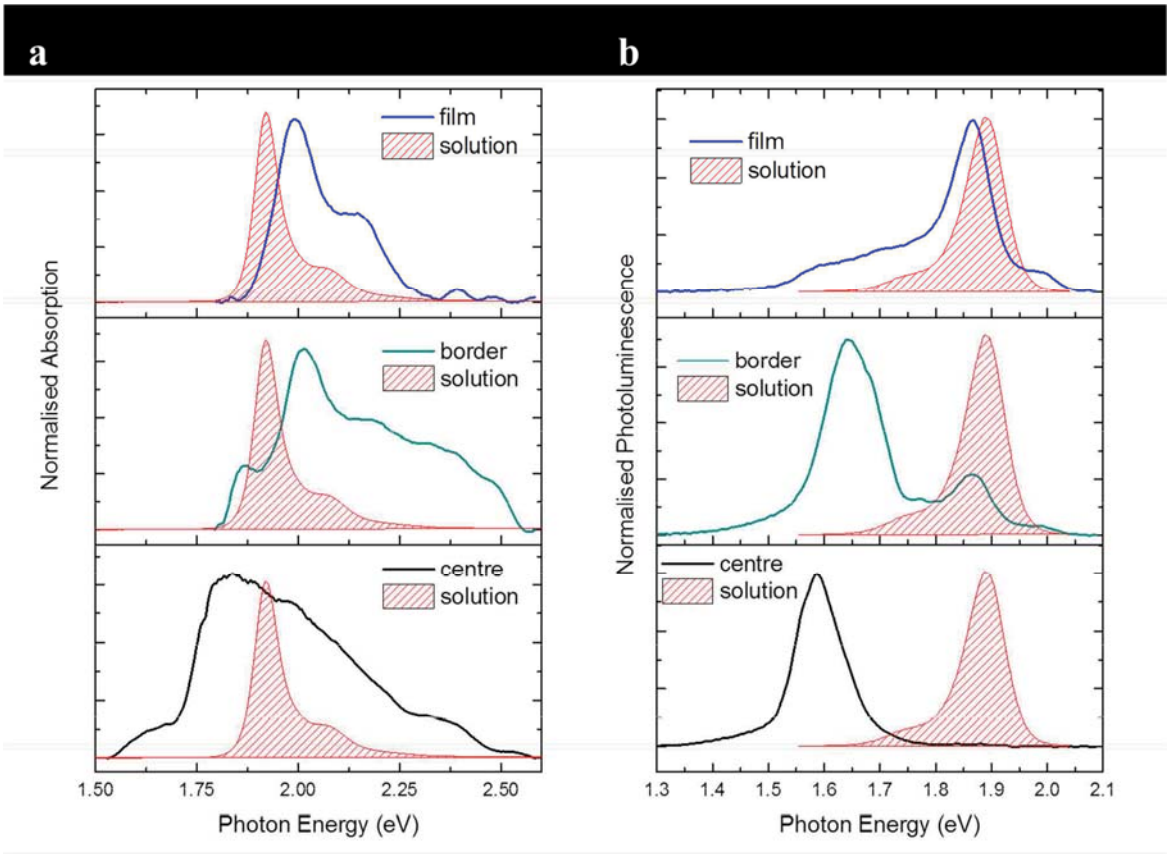

Figure 4: Absorption (a) and PL (b) spectra taken at the three different regions namely, film, aggregated-border and centre. The absorption and PL spectra of a diluted solution in ethanol of VG1 -C8 (0.14 mM) is also reported for comparison.

Conclusions

In summary, we have investigated the absorption/emission properties of a single squaraine aggregate by means of confocal microscopy, UV-Vis and PL spectroscopy. By resolving spatially and spectrally the transmission and emission of the aggregate and taking the local absorption/emission spectra, we observe that the aggregate core shows a broad absorption band centred at 1.85 eV likely originating from the presence of Davidov aggregates with allowed J- and H- configuration. Interestingly, such a region exhibits a relatively narrow emission in the NIR part of the spectrum with little overlap with the broadband absorption spectrum (Stokes shift 0.26 eV). The broad absorption spectrum, the strong and relatively narrow NIR emission alongside the small spectral overlap between absorption and PL could make these aggregates, if conveniently processed and manipulated, greatly appealing for the fabrication of efficient photovoltaic/light-emitting diodes and electrochemical cells , as well as NIR probes in biomedical applications respectively.

Conflict of interest

There are no conflicts of interest to declare.

Acknowledgements

This work is supported by the H2020 ETN SYNCHRONICS under grant agreement 643238.

References

1. J. Park, C. Barolo, F. Sauvage, N. Barbero, C. Benzi, P. Quagliotto, S. Coluccia, D. Di Censo, M. Gratzel, M. K. Nazeeruddin and G. Viscardi, *Chem Commun (Camb)*, 2012, **48**, 2782-2784.
2. J. H. Yum, P. Walter, S. Huber, D. Rentsch, T. Geiger, F. Nuesch, F. De Angelis, M. Gratzel and M. K. Nazeeruddin, *J Am Chem Soc*, 2007, **129**, 10320-10321.
3. S. Galliano, V. Novelli, N. Barbero, A. Smarra, G. Viscardi, R. Borrelli, F. Sauvage and C. Barolo, *Energies*, 2016, **9**, 486.
4. J. S. Huang, T. Goh, X. K. Li, M. Y. Sfeir, E. A. Bielinski, S. Tomasulo, M. L. Lee, N. Hazari and A. D. Taylor, *Nat Photonics*, 2013, **7**, 480-486.
5. G. Chen, H. Sasabe, T. Igarashi, Z. R. Hong and J. Kido, *J Mater Chem A*, 2015, **3**, 14517-14534.
6. T. Kinoshita, K. Nonomura, N. J. Jeon, F. Giordano, A. Abate, S. Uchida, T. Kubo, S. I. Seok, M. K. Nazeeruddin, A. Hagfeldt, M. Gratzel and H. Segawa, *Nat Commun*, 2015, **6**, 8834.
7. B. Stender, S. F. Volker, C. Lambert and J. Pflaum, *Advanced materials*, 2013, **25**, 2943-2947.
8. L. Serpe, S. Ellena, N. Barbero, F. Foglietta, F. Prandini, M. P. Gallo, R. Levi, C. Barolo, R. Canaparo and S. Visentin, *Eur J Med Chem*, 2016, **113**, 187-197.
9. R. R. Avirah, D. T. Jayaram, N. Adarsh and D. Ramaiah, *Org Biomol Chem*, 2012, **10**, 911-920.
10. G. M. Paterno, M. W. Skoda, R. Dalgliesh, F. Cacialli and V. G. Sakai, *Sci Rep*, 2016, **6**, 34609.
11. W. Wang, A. Fu, J. Lan, G. Gao, J. You and L. Chen, *Chemistry*, 2010, **16**, 5129-5137.
12. N. Narayanan, V. Karunakaran, W. Paul, K. Venugopal, K. Sujathan and K. Kumar Maiti, *Biosensors & bioelectronics*, 2015, **70**, 145-152.
13. G. Paterno, A. J. Warren, J. Spencer, G. Evans, V. G. Sakai, J. Blumberger and F. Cacialli, *J Mater Chem C*, 2013, **1**, 5619-5623.
14. G. Tregnago, M. Wykes, G. M. Paterno, D. Beljonne and F. Cacialli, *J Phys Chem C*, 2015, **119**, 11846-11851.
15. J. Mei, Y. Hong, J. W. Lam, A. Qin, Y. Tang and B. Z. Tang, *Advanced materials*, 2014, **26**, 5429-5479.
16. F. Wurthner, T. E. Kaiser and C. R. Saha-Moller, *Angewandte Chemie*, 2011, **50**, 3376-3410.
17. G. M. Lazzerini, G. M. Paternò, G. Tregnago, N. Treat, N. Stingelin, A. Yacoot and F. Cacialli, *Applied Physics Letters*, 2016, **108**, 053303.
18. K. C. Deing, U. Mayerhoffer, F. Wurthner and K. Meerholz, *Physical chemistry chemical physics : PCCP*, 2012, **14**, 8328-8334.
19. O. P. Dimitriev, A. P. Dimitriyeva, A. I. Tolmachev and V. V. Kurdyukov, *The journal of physical chemistry. B*, 2005, **109**, 4561-4567.
20. P. Chithra, R. Varghese, K. P. Divya and A. Ajayaghosh, *Chemistry, an Asian journal*, 2008, **3**, 1365-1373.
21. A. Ajayaghosh, P. Chithra, R. Varghese and K. P. Divya, *Chem Commun (Camb)*, 2008, **0**, 969-971.
22. B. Di Bartolo, *Spectroscopy of the excited state*, Springer Science & Business Media, 2012.
23. E. Fresta and R. D. Costa, *J. Mater. Chem. C*, 2017, **5**, 5643-5675.
24. R. D. Costa, E. Orti, H. J. Bolink, F. Monti, G. Accorsi and N. Armaroli, *Angewandte Chemie*, 2012, **51**, 8178-8211.
25. C. Zheng, A. R. Penmetcha, B. Cona, S. D. Spencer, B. Zhu, P. Heaphy, J. A. Cody and C. J. Collison, *Langmuir*, 2015, **31**, 7717-7726.
26. Y. Xu, Q. Liu, X. Li, C. Wesdemiotis and Y. Pang, *Chem Commun (Camb)*, 2012, **48**, 11313-11315.
27. U. Mayerhoffer, K. Deing, K. Gruss, H. Braunschweig, K. Meerholz and F. Wurthner, *Angewandte Chemie*, 2009, **48**, 8776-8779.
28. N. Jurgensen, J. Zimmermann, A. J. Morfa and G. Hernandez-Sosa, *Scientific Reports*, 2016, **6**, 36643.
29. M. D. Weber, J. E. Wittmann, A. Burger, O. B. Malc1oglu, J. Segarra-Marti, A. Hirsch, P. B. Coto, M. Bockstedte and R. D. Costa, *Adv Funct Mater*, 2016, **26**, 6736-6736.
30. Y. Shao, G. C. Bazan and A. J. Heeger, *Advanced materials*, 2007, **19**, 365-+.
31. M. D. Weber, V. Nikolaou, J. E. Wittmann, A. Nikolaou, P. A. Angaridis, G. Charalambidis, C. Stangel, A. Kahnt, A. G. Coutsolelos and R. D. Costa, *Chem Commun (Camb)*, 2016, **52**, 1602-1605.
32. S. Sreejith, J. Joseph, M. Lin, N. V. Menon, P. Borah, H. J. Ng, Y. X. Loong, Y. Kang, S. W. Yu and Y. Zhao, *ACS Nano*, 2015, **9**, 5695-5704.

33. N. Barbero, C. Magistris, J. Park, D. Saccone, P. Quagliotto, R. Buscaino, C. Medana, C. Barolo and G. Viscardi, *Organic letters*, 2015, **17**, 3306-3309.
34. G. M. Paternò, S. Galliano, N. Barbero, C. Barolo, R. Borrelli, G. Lanzani and F. Scotognella, *Proceedings of SPIE* 2017, **10101**, 101010R.
35. G. de Miguel, M. Marchena, M. Zitnan, S. S. Pandey, S. Hayase and A. Douhal, *Physical chemistry chemical physics : PCCP*, 2012, **14**, 1796-1805.
36. M. Gsanger, E. Kirchner, M. Stolte, C. Burschka, V. Stepanenko, J. Pflaum and F. Wurthner, *J Am Chem Soc*, 2014, **136**, 2351-2362.
37. E. Conterosito, I. Benesperi, V. Toson, D. Saccone, N. Barbero, L. Palin, C. Barolo, V. Gianotti and M. Milanesio, *ChemSusChem*, 2016, **9**, 1279-1289.
38. K. Y. Law, *Chemical Reviews*, 1993, **93**, 449-486.
39. A. Yassar, G. Horowitz, P. Valat, V. Wintgens, M. Hmyene, F. Deloffre, P. Srivastava, P. Lang and F. Garnier, *The Journal of Physical Chemistry*, 1995, **99**, 9155-9159.
40. D. Mobius, *Advanced materials*, 1995, **7**, 437-444.
41. R. S. Grynyov, A. V. Sorokin, G. Y. Guralchuk, S. L. Yefimova, I. A. Borovoy and Y. V. Malyukin, *The Journal of Physical Chemistry C*, 2008, **112**, 20458-20462.

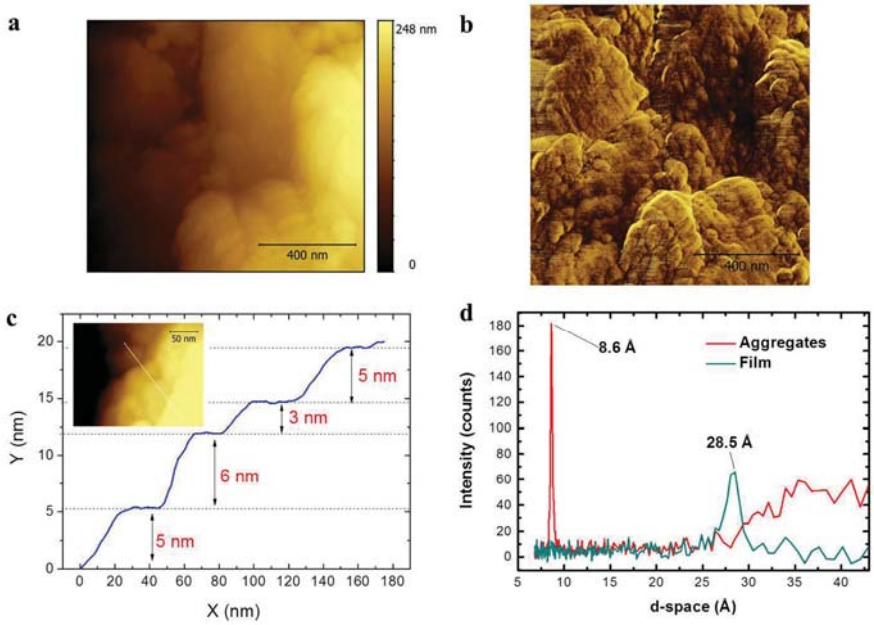

(a) AFM height and (b) phase images taken on top of a VG1-C8 aggregate; (c) AFM height-analysis of the aggregate surface; (d) out-of-plane XRD pattern of the VG1-C8 aggregate (red curve) and film (cyan curve).

497x342mm (96 x 96 DPI)

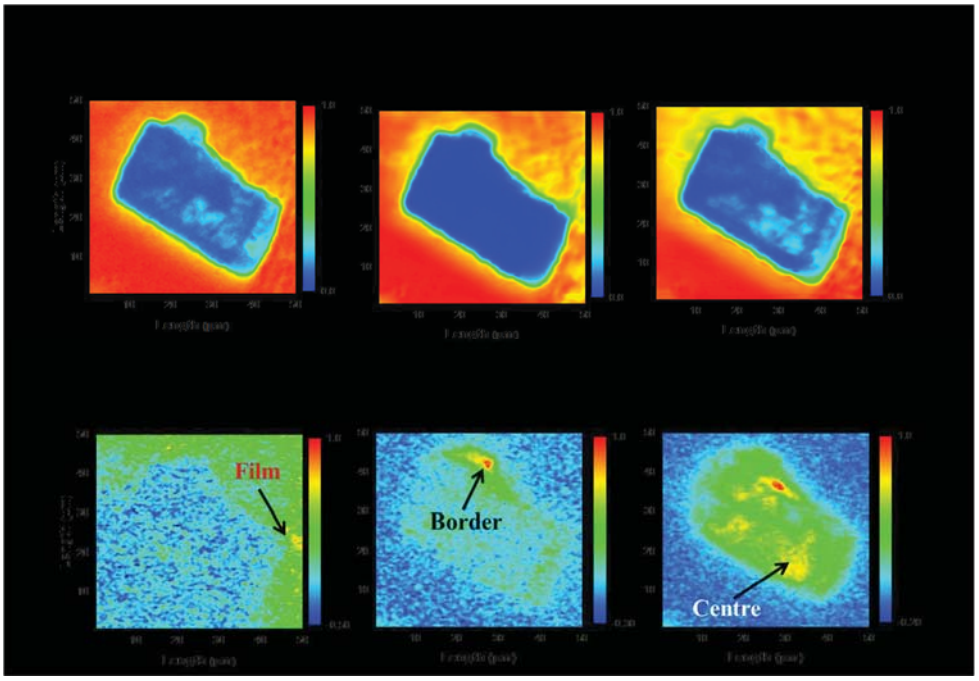

Normalised transmission (a-c) and PL (d-f) maps of the VG1 - aggregate (thickness ≈ 160 μm as measured by profilometry) and surrounding film (thickness ≈ 45 nm) . We employed BP filters to resolve spatially and highlight the different spectral contributions.

314x217mm (150 x 150 DPI)

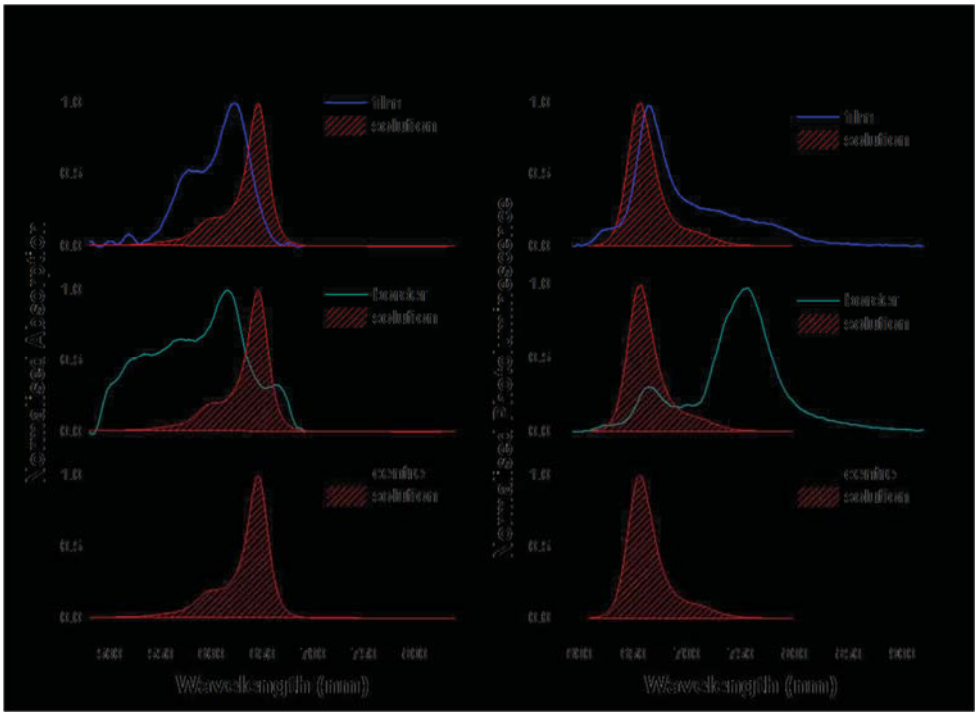

Absorption (a) and PL (b) spectra taken at the three different regions namely, film, aggregated-border and centre. The absorption and PL spectra of a diluted solution in ethanol of VG1 -es (0.14 mM) is also reported for comparison.

207x151mm (150 x 150 DPI)